The oxygen abundance gradient in M81 and the robustness of abundance determinations in H II regions

K. Z. Arellano-Córdova,★ M. Rodríguez, Y. D. Mayya and D. Rosa-González

Instituto Nacional de Astrofísica, Óptica y Electrónica (INAOE), Apdo. Postal 51 y 216, Puebla, Mexico

ABSTRACT

We study the sensitivity of the methods available for abundance determinations in H II regions to potential observational problems. We compare the dispersions they introduce around the oxygen and nitrogen abundance gradients when applied to five different sets of spectra of H II regions in the galaxy M81. Our sample contains 116 H II regions with galactocentric distances of 3 to 33 kpc, including 48 regions observed by us with the OSIRIS long-slit spectrograph at the 10.4-m Gran Telescopio Canarias telescope. The direct method can be applied to 31 regions, where we can get estimates of the electron temperature. The different methods imply oxygen abundance gradients with slopes of -0.010 to -0.002 dex kpc^{-1}, and dispersions in the range 0.06–0.25 dex. The direct method produces the shallowest slope and the largest dispersion, illustrating the difficulty of obtaining good estimates of the electron temperature. Three of the strong-line methods, C, ONS, and N2, are remarkably robust, with dispersions of $\sim$0.06 dex, and slopes in the range -0.008 to -0.006 dex kpc^{-1}. The robustness of each method can be directly related to its sensitivity to the line intensity ratios that are more difficult to measure properly. Since the results of the N2 method depend strongly on the N/O abundance ratio and on the ionization parameter, we recommend the use of the C and ONS methods when no temperature estimates are available or when they have poor quality, although the behaviour of these methods when confronted with regions that have different properties and different values of N/O should be explored.

Key words: ISM: abundances – H II regions – galaxies: abundances – galaxies: individual: M81.

1 INTRODUCTION

The analysis of the spectra of H II regions provides information about the chemical composition of the present-day interstellar medium in different kinds of star-forming galaxies and in different regions across these galaxies. The results supply fundamental input for our models of galactic chemical evolution. Oxygen, the third most abundant element, is taken as representative of the metallicity of the medium, since the oxygen abundance is the one most easily derived from the optical spectra of photoionized gas. Leaving aside the construction of photoionization models that reproduce the spectra, there are different ways to derive oxygen abundances from the observed spectra. When the spectra are deep enough to allow the measurement of the weak lines needed for the determination of electron temperatures, such as [O III] λ4363 or [N II] λ5755, we can use the direct method to derive the O^+ and O^{++} abundances, and obtain the total oxygen abundance by adding these ionic abundances.

On the other hand, when the temperature-sensitive lines are not detected, one must resort to alternative methods that are based on the intensities of the strongest lines, the so-called strong-line methods. These methods are calibrated using grids of photoionization models or samples of H II regions that have estimates of the electron temperature (the empirical methods).

The strongest lines in the optical spectra of H II regions that are usually used by strong-line methods are [O II] λ3727, [O III] $\lambda\lambda$4959, 5007, [N II] $\lambda\lambda$6548 + 84, [S II] $\lambda\lambda$6717 + 31, Hα, and Hβ. Different methods use different combinations of line ratios involving these lines and, although a large variety of methods are available, it is important to consider the procedures that have been used to calibrate them, and whether the samples of observed objects or photoionization models used for the calibration cover the same physical properties as the H II regions to which the method will be applied (Stasińska 2010). In general, different methods and different calibrations of the same method will lead to different results.

It is not easy to construct grids of photoionization models that reproduce well enough the main characteristics of the observed H II regions so that they can be used to calibrate the strong-line

★ E-mail: karlaz@inaoep.mx

methods (Dopita et al. 2006; Stasińska 2008). This might explain the fact that the abundances derived with methods based on this type of calibration differ from those derived with empirical methods (Kewley & Ellison 2008; López-Sánchez & Esteban 2010). As an example of the complications that arise when defining the input parameters of photoionization models, we do not have much information about the properties of dust grains inside H II regions (see e.g. Ochsendorf & Tielens 2015) and they have important effects on the emitted spectrum (van Hoof et al. 2004), especially at high metallicities. Empirical methods also have their problems: it is difficult to measure the lines needed for temperature determinations in metal-rich regions, the electron temperatures estimated for these regions can introduce important biases in the abundance determinations (Stasińska 2005), and if, as suggested by several authors, there are temperature fluctuations in H II regions which are larger than those predicted by photoionization models, they can lead to lower abundances than the real ones at any metallicity (e.g. Peña-Guerrero, Peimbert & Peimbert 2012).

If one excludes from the samples high-metallicity objects, and if temperature fluctuations turn out to be not much higher than the ones expected from photoionization models, it can be argued that empirical calibrations of the strong-line methods should be preferred because they are based on a lower number or assumptions, although photoionization models can provide much insight on the explanations behind the behaviour and applicability of the strong-line methods. One important question is how well strong-line methods can be expected to do. Grids of photoionization models can be used to show that strong-line methods work because the metallicity of most H II regions is strongly related to the effective temperature of the ionizing radiation and to the ionization parameter of the region[1] (Dopita et al. 2006; Stasińska 2008). This implies that strong-line methods will not work properly when applied to regions that do not follow this general relation due to variations in their star formation histories, ages, or chemical evolution histories (Stasińska 2010). The direct method is expected to work better since it is based on a smaller number of assumptions, and when observations of H II regions are presented in any publication, it is usually described as an achievement to detect the weak lines that allow a temperature determination.

However, the measurement of the weak, temperature-sensitive, lines can be affected by large uncertainties when these lines have a low signal-to-noise ratio in the nebular spectrum. When the oxygen abundances are derived with the direct method using temperature estimates based on these lines, the results will also have large uncertainties. The calibration of strong-line methods using these oxygen abundances can be affected by the large uncertainties, but this problem can be alleviated by a careful selection of calibration samples trying to have small, randomly distributed, uncertainties, and by cleaning up the samples excluding the outliers, since it can be assumed that they depart from the relation implied by the rest of the sample either because they have different properties or because their line intensities have large uncertainties. In principle the average behaviour of these samples could allow good calibrations of strong-line methods which might then show lower dispersions than the results of the direct method when applied to objects in the calibration sample or to objects that have the average properties of the calibration sample. In these cases, strong-line methods will be more robust than the direct method.

[1] The number of ionizing photons per atom arriving to the inner face of the ionized region.

The measurement of the intensities of the strong lines used by the strong-line methods should present less problems. However, there are observational effects that introduce uncertainties in all the measurements of line intensity ratios, effects that are not necessarily included in the estimated uncertainties, namely, atmospheric differential refraction leading to the measurement of different lines at different spatial positions, the incorrect extraction of 1D spectra from tilted 2D spectra, undetected absorption features beneath the emission lines, problems with the estimation of the continuum or with deblending procedures, the presence of unnoticed cosmic rays, or any bias introduced by the flux calibration or the extinction correction. Some of the line ratios used by strong-line methods will be more sensitive to these effects, making these methods less robust than others that are based on less-sensitive line ratios. Moreover, since the line ratios used as temperature diagnostics can be very sensitive to these observational problems, the results of the direct method might be less robust than those derived with strong-line methods even when the weak temperature-sensitive lines are measured with a good signal-to-noise ratio.

One way to infer the robustness of the methods used for abundance determinations in the presence of observational problems is to compare their performance when they are used to estimate metallicity gradients in galaxies. The observational problems are likely to introduce dispersions around an existing gradient that can be interpreted as azimuthal abundance variations. If any of the methods implies significantly lower dispersions, it seems reasonable to assume that azimuthal variations must be lower than the estimated dispersions, and hence that the method is behaving in a more robust way. Since spectra obtained by different authors are likely to be affected by various observational problems in different amounts, the robustness of each method to observational effects can be inferred from the dispersions around the gradient implied by the method when using spectra observed by different authors in the same galaxy. Methods that show significantly lower dispersions can then be inferred to be more robust.

Here we present an analysis of the oxygen abundance gradient in M81, using this galaxy as a case study of the robustness of some of the methods used for abundance determinations in H II regions. We will explore the behaviour of methods that have been calibrated using large samples of H II regions that have temperature determinations. M81 is an ideal candidate for this study, since it is a nearby spiral galaxy, at a distance of 3.63 ± 0.34 Mpc (Freedman et al. 2001). This galaxy belongs to an interacting group of galaxies and has well-defined spiral arms that contain a large number of H II regions. The oxygen abundance gradient of M81 has been calculated in different studies using several methods (Stauffer & Bothun 1984; Garnett & Shields 1987; Pilyugin, Vílchez & Contini 2004; Stanghellini et al. 2010, 2014; Patterson et al. 2012; Pilyugin, Grebel & Kniazev 2014). These works find slopes that go from -0.093 to -0.011 dex kpc^{-1}, and some of them include H II regions where it is possible to measure the electron temperature and calculate the metallicity with the direct method.

This paper is structured as follows: in Section 2 we describe our observations, which were obtained with the Gran Telescopio Canarias (GTC), the data reduction, the sample selection, the measurement of the line intensities, and the reddening corrections; in Section 3 we describe the methods we apply to calculate the physical conditions and chemical abundances of the sample of H II regions; in Section 4 we present the results of this analysis, and the implied metallicity gradients, using our data and other observations from the literature; in Section 5 we discuss the scatter around the metallicity

Table 1. Log of the observations.

Slit ID	R.A. (J2000)	Dec. (J2000)	Exposure times (s)	P.A. (°)	Airmass
P1	09:54:38	+69:05:48	3×900	171	1.3
P2	09:54:52	+69:08:11	3×900	6	1.3
P3	09:55:37	+69:07:46	3×900	123	1.4
P4	09:55:46	+69:07:48	3×900	105	1.5
P5	09:55:48	+69:04:53	3×900	127	1.4

gradient implied by the different methods; and finally, in Section 6, we summarize our results and present our conclusions.

2 OBSERVATIONS AND DATA REDUCTION

Spectroscopic observations (programme GTC11-10AMEX, PI: DRG) were carried out using the long-slit spectrograph of the OSIRIS instrument at the 10.4-m GTC telescope in the Observatorio del Roque de los Muchachos (La Palma, Spain). We used the five slit positions listed in Table 1, with a slit width of 1 arcsec and length of 8 arcmin. Table 1 provides the central positions of the slits, the exposure times we used, the slit position angles (P.A.), and the airmasses during the observations. We obtained three exposures of 900 s at each slit position using the R1000B grism, which allowed us to cover the spectral range 3630–7500 Å with a spectral resolution of ∼7 Å full width at half-maximum. The observations were acquired on 2010 April 5–7 when the seeing was ∼1 arcsec. The detector binning by 2 pixels in the spatial dimension provided a scale of 0.25 arcsec pixel^{-1}. The airmasses were in the range 1.3–1.5 and, at these values, departures from the parallactic angle can introduce light losses at some wavelengths due to differential atmospheric refraction (Filippenko 1982). In our observations, the differences between the position angle and the parallactic angle go from 8° to 23°. Although small, the differences imply that we might be losing some light in the blue, especially for the few objects with sizes around 1 arcsec observed with slit positions P1 and P2. This is one of the possible observational problems that we listed in Section 1, and the combined effects of these problems are explored in our analysis.

The data were reduced using the tasks available in the IRAF[2] software package. The reduction process included bias subtraction, flat-field and illumination correction, sky subtraction, wavelength calibration, and flux calibration using the standard star Feige 34. The final spectra result from the median of the three exposures obtained at each slit position.

The slit positions were selected to pass through some of the brightest stellar compact clusters in the catalogue of Santiago-Cortés, Mayya & Rosa-González (2010) for M81. These observations are part of a large-scale program dedicated to study the star formation in this galaxy (Mayya et al. 2013). Here we use them to study the chemical abundances and the abundance gradient provided by H II regions in M81. We extracted spectra using the task APALL of IRAF for each knot of ionized gas that we found along the five slits. There were two or three bright stellar clusters in each slit and we used the one closest to each ionized knot to trace the small changes of position of the stellar continuum in the CCD. We fitted polynomial functions to these traces and used them as a reference

to extract the spectrum of the knots. The size of the apertures goes from 4 to 28 pixels (1 to 7 arcsec). The final sample consists of 48 H II regions located in the disc of M81.

Fig. 1 shows the UV image of M81 from *GALEX* (Galaxy Evolution Explorer) with our slit positions superposed. We also show boxes around the regions where we could extract spectra for several knots of ionized gas. One to eight knots were extracted in each of the boxes shown in Fig. 1. The boxes are tagged as P*n-m*, where *n* identifies the slit and *m* the box along this slit. We identify the knots with numbers going from 1 to 48, starting with the first knot in box P1-1 and ending with the knots in P5-2, moving from South to North in the slits P1 and P2 and from East to West for the slits P3, P4, and P5. We also show an inset in Fig. 1 with a cut in the spatial direction along one of the columns with Hα emission in our 2D spectra for box P3-3, illustrating the procedure we followed for selecting the ionized knots. Fig. 2 shows two examples of the extracted spectra, one with a high signal-to-noise ratio (region 1) and a second one with a low signal-to-noise ratio (region 22).

2.1 Line measurements

Line intensities were measured using the SPLOT routine of IRAF by integrating the flux above the continuum defined by two points on each side of the emission lines. We fitted Gaussian profiles for those lines that appear blended. The errors in the line intensities were calculated using the expression (Tresse et al. 1999):

$$\sigma_I = \sigma_c D \sqrt{2 N_{pix} + \frac{EW}{D}}, \qquad (1)$$

where D is the spectral dispersion in Å per pixel, σ_c is the mean standard deviation per pixel of the continuum on each side of the line, N_{pix} is the number of pixels covered by the line and EW is the equivalent width. We corrected the Balmer line intensities for the effects of stellar absorption by assuming absorption equivalent widths of 2 Å (McCall, Rybski & Shields 1985). The correction is small for most of our regions, with changes in the Hα and Hβ intensities below 7 and 10 per cent, respectively, but it is significant for six regions. In four of them (regions 7, 42, 43, and 44) it increases the intensity of Hβ by just 12–14 per cent, but regions 6 and 14 have increments of 72 and 27 per cent, respectively. The effects of these changes on our results are described in Section 4.1.

The emission lines were corrected for extinction assuming an intrinsic line ratio of Hα/Hβ = 2.86, suitable for T_e = 10 000 K and n_e = 100 cm^{-3} (Osterbrock & Ferland 2006), since we find similar values for the physical conditions in our objects. We used the extinction law of Cardelli, Clayton & Mathis (1989) with a ratio of total to selective extinction in V and $B - V$ of R_V = 3.1.

To correct for reddening each emission line ratio, we use the expression:

$$\frac{I(\lambda)}{I(H\beta)} = \frac{I_0(\lambda)}{I_0(H\beta)} 10^{-c(H\beta)[f(\lambda)-1]} \qquad (2)$$

where $I(\lambda)/I(H\beta)$ is the observed line intensity ratio, $I_0(\lambda)/I_0(H\beta)$ is the reddening-corrected ratio, $c(H\beta)$ is the reddening coefficient, and $f(\lambda)$ is the extinction law normalized to Hβ.

Tables 2 and 3, whose full versions are available online, show the values of the extinction coefficients and the observed and reddening-corrected line ratios for each region. We also provide for each region the extinction corrected $I(H\beta)$ in Table 2. The final errors are the result of adding quadratically the uncertainties in the measured intensities, 4 per cent as our estimate of the uncertainty in the flux

---

[2] IRAF is distributed by the National Optical Astronomy Observatory, which is operated by the Association of Universities for Research in Astronomy, Inc., under cooperative agreement with the National Science Foundation.
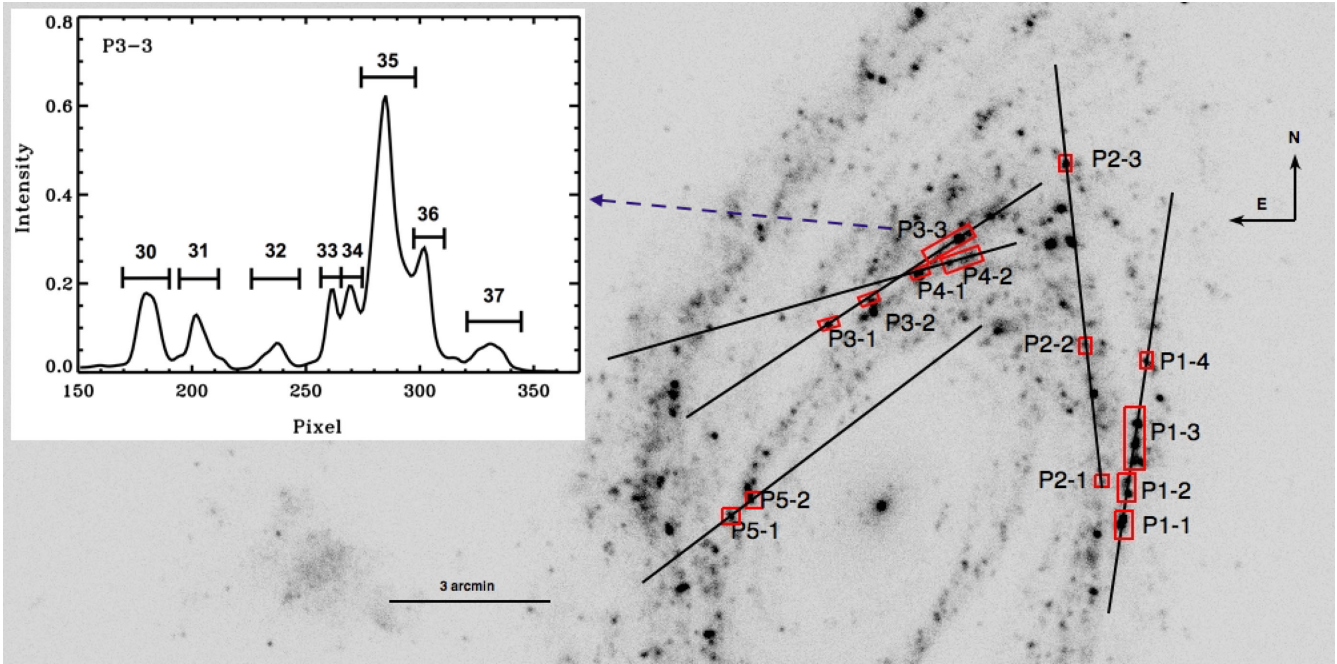
Figure 1. UV image of M81 from *GALEX* showing the slit positions listed in Table 1. The boxes show the locations of the ionized knots in our sample. The inset shows a cut in the spatial direction along the Hα emission line for box P3-3. We identify in the inset the knots of ionized gas whose spectra we extracted in this region.
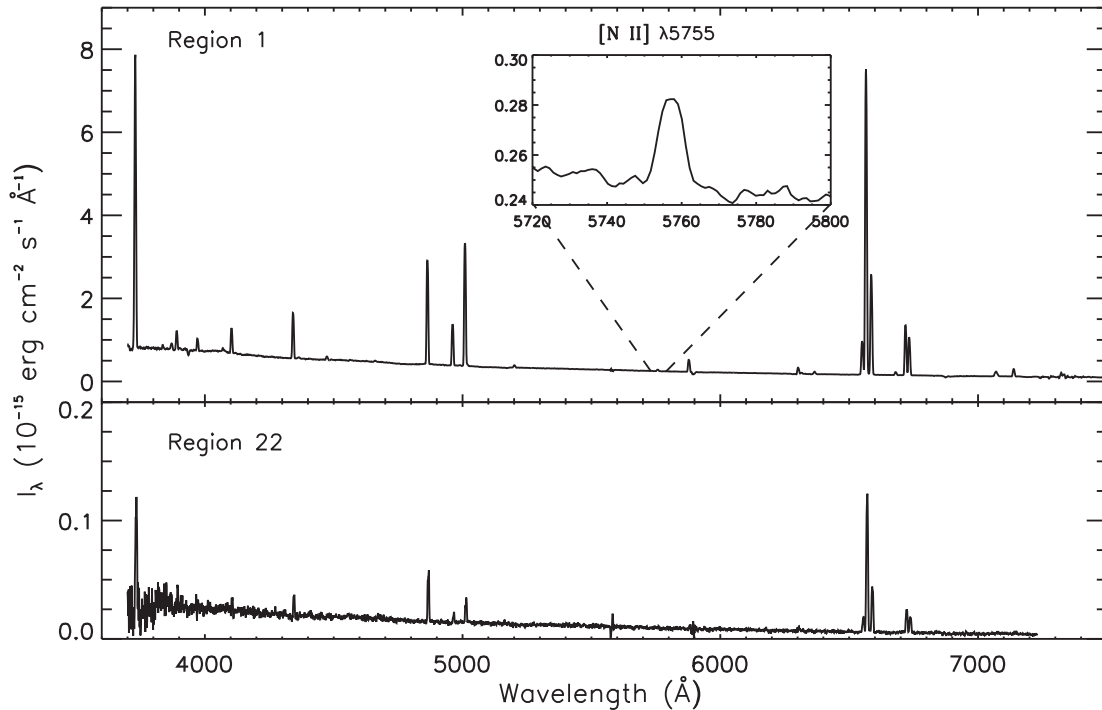
Figure 2. Spectra of two of our observed regions. Region 1 has one of the spectra with the highest signal-to-noise ratios; region 22 has one of the lowest signal-to-noise ratios. The inset shows our detection of the temperature-sensitive line [N II] λ5755 in region 1.

calibration, and the uncertainty in the reddening correction. The values we find for $c(H\beta)$ are in the range 0–0.51, in agreement with the values found by Patterson et al. (2012) for several H II regions in M81, $c(H\beta) = 0.07$–0.43 but significantly lower than the values obtained by Stanghellini et al. (2010) for H II regions in this galaxy, $c(H\beta) = 0.48$–0.92.

3 PHYSICAL CONDITIONS AND OXYGEN ABUNDANCES

3.1 The direct method

We could measure the temperature-sensitive [N II] λ5755 line in 12 of the 48 H II regions in our sample, where it shows a well-defined

Table 2. The extinction coefficients $c(H\beta)$ and the reddening-corrected intensities for $H\beta$. The full table for the 48 regions is available online.

Region	$c(H\beta)$	Error	$I(H\beta)$ (erg cm^{-2} s^{-1})
1	0.14	0.07	2.75×10^{-14}
2	0.35	0.08	5.95×10^{-15}
3	0.39	0.07	8.20×10^{-15}
4	0.00	0.10	5.51×10^{-16}
5	0.06	0.08	1.37×10^{-15}
6	0.00	0.09	2.84×10^{-16}
7	0.28	0.08	7.87×10^{-16}
8	0.00	0.07	3.60×10^{-15}
9	0.25	0.09	9.44×10^{-16}
10	0.35	0.08	1.25×10^{-14}

Table 3. Some of the observed and reddening-corrected line ratios, normalized to $I(H\beta) = 100$, for region 1. The error is expressed as a percentage of the reddening-corrected values. The full table with the line intensities for the 48 regions is available online.

Region	$\lambda(\text{Å})$	ID	$I(\lambda)$	$I_0(\lambda)$	Error (per cent)
1	3727	[O II]	266	306	8
1	4101	Hδ	21.4	23.7	7
1	4341	Hγ	41.2	44.2	6
1	4471	He I	3.3	3.5	8
1	4861	Hβ	100.0	100.0	5
1	4959	[O III]	40.0	39.5	5
1	5007	[O III]	120.1	118.1	5
1	5200	[N I]	2.5	2.5	8
1	5755	[N II]	1.4	1.3	9
1	5876	He I	11.8	10.8	6

profile with a S/N ≥ 3.6 (see e.g. Fig. 2). This allows us to use the so-called direct method to derive the oxygen abundances, which is, in principle, the most reliable method. The [O III] $\lambda4363$ auroral line was marginally detected in two regions with a noisy profile. The line can be affected by imperfect sky subtraction of the Hg $\lambda4358$ sky line, and we decided not to use it.

In order to calculate the physical conditions and the ionic oxygen abundances in these 12 H II regions, we use the tasks available in the NEBULAR package of IRAF, originally based on the calculations of De Robertis, Dufour & Hunt (1987) and Shaw & Dufour (1995). We adopted the following atomic data: the transition probabilities of Zeippen (1982) for O$^+$, Wiese, Fuhr & Deters (1996) and Storey & Zeippen (2000) for O^{++}, Wiese et al. (1996) for N$^+$ and Mendoza & Zeippen (1982) for S$^+$; and the effective collision strengths of Pradhan et al. (2006) for O$^+$, Aggarwal & Keenan (1999) for O^{++}, Lennon & Burke (1994) for N$^+$, and Keenan et al. (1996) for S$^+$.

We use the line intensity ratio [S II] $\lambda6717/\lambda6731$ to calculate the electron density, n_e, and [N II] $(\lambda6548 + \lambda6583)/\lambda5755$ to calculate the electron temperature. The [S II] ratio could be measured in all the regions, and we used $T_e = 10\,000$ K to derive n_e in those regions where the [N II] $\lambda5755$ line was not available. We obtain $n_e \lesssim 100$ cm^{-3} in most of the regions. At these densities, the [S II] diagnostic is not very sensitive to density variations (Osterbrock & Ferland 2006) and, in fact, some of the regions have a line ratio that lies above the range of expected values. However, all the [S II] line ratios but two are consistent within one sigma with $n_e \lesssim 100$ cm^{-3} and, since for these values of n_e the derived ionic abundances show a slight dependence on density, we use $n_e = 100$ cm^{-3} in all our calculations. On the other hand, the upper level of the [N II] $\lambda5755$

line can be populated by transitions resulting from recombination, leading to an overestimate of the electron temperature (Rubin 1986). We used the expression derived by Liu et al. (2000) to estimate a correction for this contribution, but found that the effect is very small in our objects, $\lesssim40$ K in T_e, so that it is safe to ignore this correction. The values derived for n_e and T_e([N II]) are listed in Table 4, where we use ':' to identify the most uncertain values of n_e. Table 4 also gives for all the objects in our sample the number that we use for identification purposes, the coordinates of the region, the slit and box where the spectra were extracted, the angular sizes of the extracted regions, their galactocentric distances (see Section 4), and their oxygen and nitrogen abundances derived with the methods described below.

We adopt a two-zone ionization structure characterized by T_e([N II]) in the [O II] emitting region and by T_e([O III]) in the [O III] emitting region, where the value of T_e([O III]) is obtained using the relation given by Campbell, Terlevich & Manlike (1986, see also Garnett 1992):

$$T_e([\text{N II}]) \simeq T_e([\text{O II}]) = 0.7\,T_e([\text{O III}]) + 3000\text{ K}, \qquad (3)$$

which is based on the photoionization models of Stasińska (1982). This relation is widely used (see e.g. Bresolin 2011; Patterson et al. 2012; Pilyugin, Grebel & Mattson 2012) and is similar to the one obtained from good-quality observations of H II regions (Esteban et al. 2009).

The ionic oxygen abundances are derived using the physical conditions described above and the intensities of [O II] $\lambda3727$ and [O III] $\lambda\lambda4959, 5007$ with respect to $H\beta$. The final values of the oxygen abundances can be obtained by adding the contribution of both ions: O/H = O$^+$/H$^+$ + O^{++}/H$^+$. The N abundance is calculated using the [N II] $\lambda\lambda6548 + 84$ lines and the assumption that N/O $\simeq$ N$^+$/O$^+$.

3.2 Strong-line methods

When the emission lines needed to derive the electron temperature are too weak to be observed, it is still possible to estimate chemical abundances with the so-called strong-line methods. These methods are based on the intensities of lines that can be easily measured, such as [O II] $\lambda3727$, [O III] $\lambda5007$, or [N II] $\lambda6584$, and are calibrated using photoionization models or observational data of H II regions that include measurements of the electron temperature. The two approaches often lead to different results (see e.g. Kewley & Ellison 2008), but we will not enter here into a discussion of which one yields the better estimates; we will use the empirical methods just because they provide the simplest approach to the problem. We have selected some of the empirical calibrations that are based on the largest numbers of H II regions: the P method of Pilyugin & Thuan (2005), the ONS method of Pilyugin, Vílchez & Thuan (2010), the C method of Pilyugin et al. (2012) and the O3N2 and N2 methods calibrated by Marino et al. (2013). The methods use initial samples of around 100–700 H II regions that have temperature measurements, although in some cases different criteria are applied in order to select more adequate or more reliable subsamples. All these methods provide estimates of the oxygen abundance, whereas nitrogen abundances can only be obtained with the ONS and C methods. We describe the methods below.

3.2.1 The P method

Some of the most widely used strong-line methods are based on the parameter $R_{23} = I([\text{O II}]\lambda3727)/I(H\beta) + I([\text{O III}]\lambda\lambda4959,$

Table 4. Coordinates, sizes, galactocentric distances, physical conditions and oxygen abundances for the 48 H II regions in our sample. The oxygen abundances have been derived with the direct method (T_e) and five strong-line methods (P, ONS, C, O3N2, and N2).

ID	Box	RA (J2000)	Dec. (J2000)	Size (arcsec)	R (kpc)	n_e (cm^{-3})	T_e([N II]) (K)	(T_e)	(P)	(ONS)	(C)	(O3N2)	(N2)
1	P1-1	09:54:43	+69:03:39	5.1	8.9	115 ± 6	10100^{+500}_{-400}	$8.13^{+0.06}_{-0.07}$	8.33	8.45	8.43	8.42	8.53
2		09:54:43	+69:03:33	2.1	8.9	–	–	$8.09^{+0.08}_{-0.09}$	8.22	8.45	8.52	8.45	8.54
3		09:54:43	+69:03:31	2.5	8.9	27 ± 21	–	–	8.42	8.48	8.49	8.39	8.59
4		09:54:43	+69:03:24	2.0	9.0	–	–	–	8.08	8.40	8.44	8.43	8.52
5	P1-2	09:54:41	+69:04:23	4.6	8.7	–	10900^{+1700}_{-1000}	$7.96^{+0.16}_{-0.20}$	8.22	8.46	8.55	8.49	8.56
6		09:54:42	+69:04:08	1.5	8.8	314:	–	–	8.53	8.52	8.47	8.41	8.48
7		09:54:42	+69:04:06	2.6	8.8	–	–	–	8.30	8.46	8.49	8.43	8.50
8	P1-3	09:54:39	+69:05:01	2.9	8.7	23:	9400^{+800}_{-600}	$8.17^{+0.11}_{-0.12}$	8.43	8.49	8.46	8.45	8.53
9		09:54:40	+69:04:58	2.0	8.7	–	–	–	8.27	8.57	8.57	8.58	8.54
10		09:54:40	+69:04:49	6.2	8.7	84 ± 22	10400^{+500}_{-400}	8.13 ± 0.07	8.33	8.44	8.40	8.40	8.55
11		09:54:40	+69:04:40	5.1	8.7	19:	–	–	8.29	8.50	8.50	8.52	8.57
12		09:54:40	+69:05:06	3.7	8.7	–	10600^{+1800}_{-1000}	$8.08^{+0.16}_{-0.20}$	8.21	8.43	8.51	8.43	8.53
13		09:54:40	+69:05:10	1.0	8.7	2:	–	–	8.24	8.59	8.56	8.58	8.54
14		09:54:40	+69:05:13	2.3	8.7	50:	–	–	8.06	8.51	8.53	8.58	8.59
15		09:54:40	+69:05:24	5.4	8.7	3:	–	–	8.28	8.58	8.56	8.57	8.52
16	P1-4	09:54:38	+69:06:38	4.9	8.5	–	–	–	8.44	8.53	8.52	8.53	8.56
17	P2-1	09:54:47	+69:04:25	3.1	7.7	–	13300^{+1800}_{-1200}	$7.70^{+0.11}_{-0.12}$	8.51	8.50	8.34	8.27	8.39
18	P2-2	09:54:50	+69:06:56	5.8	6.6	117:	–	–	8.27	8.44	8.50	8.42	8.52
19	P2-3	09:54:54	+69:10:23	1.7	7.9	–	–	–	8.60	8.37	8.60	8.56	8.31
20		09:54:54	+69:10:21	1.4	7.8	2:	–	–	8.34	8.52	8.52	8.51	8.52
21		09:54:54	+69:10:19	5.1	7.8	–	–	–	8.51	8.40	8.52	8.49	8.41
22		09:54:54	+69:10:17	1.8	7.8	–	–	–	8.38	8.51	8.46	8.50	8.54
23		09:54:54	+69:10:23	6.0	7.9	14:	–	–	8.24	8.42	8.37	8.33	8.57
24	P3-1	09:55:44	+69:07:19	1.4	5.4	18 ± 8	10500^{+900}_{-700}	$7.95^{+0.11}_{-0.13}$	8.15	8.54	8.54	8.56	8.54
25		09:55:45	+69:07:18	1.6	5.5	34:	–	–	8.10	8.50	8.53	8.53	8.55
26		09:55:45	+69:07:18	2.3	5.5	2:	–	–	8.28	8.70	8.58	8.65	8.49
27	P3-2	09:55:36	+69:07:48	1.6	5.1	36:	–	–	8.60	8.55	8.47	8.47	8.57
28		09:55:36	+69:07:47	2.6	5.1	–	–	–	8.61	8.56	8.47	8.45	8.51
29		09:55:35	+69:07:50	1.0	5.1	–	–	–	8.73	8.63	8.49	8.49	8.53
30	P3-3	09:55:21	+69:08:40	3.9	5.4	–	–	–	8.35	8.50	8.55	8.50	8.53
31		09:55:20	+69:08:44	5.3	5.4	–	–	–	8.28	8.62	8.58	8.61	8.53
32		09:55:18	+69:08:48	4.4	5.5	–	–	–	8.26	8.44	8.33	8.31	8.55
33		09:55:17	+69:08:51	1.5	5.5	–	9000^{+900}_{-600}	$8.13^{+0.14}_{-0.17}$	8.35	8.54	8.56	8.55	8.55
34		09:55:17	+69:08:52	1.9	5.6	16:	–	–	8.52	8.53	8.50	8.47	8.52
35		09:55:17	+69:08:55	4.1	5.6	16:	8200^{+700}_{-600}	$8.46^{+0.15}_{-0.16}$	8.57	8.53	8.49	8.39	8.49
36		09:55:16	+69:08:59	2.0	5.6	–	8400^{+1000}_{-600}	$8.39^{+0.15}_{-0.17}$	8.52	8.51	8.49	8.42	8.51
37		09:55:15	+69:09:01	5.2	5.7	–	–	–	8.32	8.64	8.59	8.61	8.53
38	P4-1	09:55:25	+69:08:19	7.2	5.1	13:	–	–	8.35	8.54	8.55	8.55	8.56
39		09:55:26	+69:08:17	2.5	5.1	18 ± 8	–	–	8.47	8.56	8.56	8.54	8.55
40	P4-2	09:55:19	+69:08:29	2.5	5.1	26 ± 6	$10\,000^{+400}_{-300}$	8.11 ± 0.05	8.53	8.52	8.48	8.34	8.46
41		09:55:17	+69:08:31	3.0	5.2	–	–	–	8.47	8.48	8.44	8.41	8.54
42		09:55:14	+69:08:34	2.5	5.2	6:	–	–	8.45	8.57	8.56	8.55	8.55
43		09:55:19	+69:08:29	1.5	5.1	–	–	–	8.60	8.62	8.57	8.49	8.40
44		09:55:22	+69:08:25	2.7	5.1	–	–	–	8.16	8.39	8.37	8.47	8.69
45	P5-1	09:56:05	+69:03:44	3.2	5.4	3:	–	–	8.52	8.58	8.55	8.51	8.50
46		09:56:05	+69:03:45	1.0	5.4	–	–	–	8.31	8.58	8.57	8.58	8.55
47	P5-2	09:56:01	+69:04:00	2.6	4.8	16:	–	–	8.56	8.53	8.53	8.44	8.51
48		09:55:60	+69:04:03	2.0	4.8	–	–	–	8.39	8.56	8.57	8.57	8.57

5007)/I(Hβ), first introduced by Pagel et al. (1979). There are many different calibrations of this method, and they can lead to oxygen abundances up to 0.5 dex above those obtained from the direct method (Kennicutt, Bresolin & Garnett 2003). Here we use the calibration of Pilyugin & Thuan (2005), which is based on a large sample of H II regions that have temperature measurements. This calibration is called the P method because it uses as a second parameter in the abundance determination an estimate of the hardness of the ionizing radiation, $P = I$([O III]$\lambda\lambda4959, 5007)/(I$([O III] $\lambda\lambda4959, 5007) + I$([O II]$\lambda3727$)), as proposed by Pilyugin (2001a,b). Ac-

cording to Pilyugin & Thuan (2005), this method provides oxygen abundances that differ by less than 0.1 dex from the values obtained with the direct method.

The main problem with the methods based on R_{23} is that the relation of this parameter with $12 + \log$(O/H) is double valued: the same value of R_{23} can lead to two different values of the oxygen abundance and one must find a procedure to break this degeneracy. Following Kewley & Ellison (2008), we use $\log$(I([N II]$\lambda6584)/I$([O II] $\lambda3727$)) $= -1.2$ as the dividing line between low- and high-metallicity objects.

Downloaded from http://mnras.oxfordjournals.org/ at Instituto Nacional de Astrofísica, Optica y Electronica on December 12, 2016

3.2.2 The ONS method

The ONS method, proposed by Pilyugin et al. ([2010](#)), uses the relative intensities of the lines [O II] λ3727, [O III] $\lambda\lambda$4959, 5007, [N II] λ6548 + 84, [S II] λ6717 + 31, and Hβ. Pilyugin et al. ([2010](#)) classify the H II regions as cool, warm, or hot depending on the relative intensities of the [N II], [S II] and Hβ lines, and provide different formulae that relate the oxygen and nitrogen abundances to several line ratios for each case. Pilyugin et al. ([2010](#)) find that the method shows very good agreement with the abundances they derive using the direct method, with root mean square differences of 0.075 dex for the oxygen abundance and 0.05 dex for the nitrogen abundance. Li, Bresolin & Kennicutt ([2013](#)) find similar differences with the direct method for their sample H II regions, around 0.09 dex in the oxygen abundance.

3.2.3 The C method

The counterpart method or C method of Pilyugin et al. ([2012](#)) is based on the assumption that H II regions that have similar intensities in their strong emission lines have similar physical properties and chemical abundances. The method uses a data base of 414 reference H II regions that are considered to have good estimates of the electron temperature, and looks for objects that have values which are similar to the ones observed in the H II region under study for several line ratios involving the lines [O II] λ3727, [O III] λ5007, [N II] λ6584, [S II] λ6717 + 31, and Hβ. The method then finds a relation between the oxygen or nitrogen abundance and the values of these line intensity ratios for these objects, which is then applied to derive the oxygen abundance of the observed H II region. Pilyugin et al. ([2012](#)) estimate that if the errors in the line intensity ratios are below 10 per cent, the method leads to abundance uncertainties of less than 0.1 dex in the oxygen abundance, and 0.15 dex in the nitrogen abundance.

3.2.4 The O3N2 and N2 methods

The O3N2 and N2 methods were proposed by Alloin et al. ([1979](#)) and Storchi-Bergmann, Calzetti & Kinney ([1994](#)), respectively. They use the line ratios:

$$\text{O3N2} = \log\left(\frac{I([\text{O III}]\lambda5007)/I(\text{H}\beta)}{I([\text{N II}]\lambda6584)/I(\text{H}\alpha)}\right) \qquad (4)$$

and

$$\text{N2} = \log(I([\text{N II}]\lambda6584)/I(\text{H}\alpha)). \qquad (5)$$

These methods are not sensitive to the extinction correction or flux calibration and have been widely used. However, the O3N2 method cannot be used at low metallicities, the N2 method can be affected by shocks or the presence of an AGN in nuclear H II regions (Kewley & Dopita [2002](#)), and both methods are very sensitive to the degree of ionization of the observed region and to its value of N/O. This might explain the large dispersions usually found in their calibration, although this could also be due to the selection of the calibration sample. We will use the calibrations of Marino et al. ([2013](#)) for these two methods that are based on H II regions with temperature measurements. The root mean square differences between the oxygen abundances derived with these methods and those derived with the direct method for the objects used by Marino et al. ([2013](#)) are 0.16 dex (N2 method) and 0.18 dex (O3N2 method).

4 RESULTS

4.1 Oxygen abundances and the oxygen abundance gradient

Table [4](#) shows the oxygen abundances derived for the 48 regions in our sample using the methods described above. The uncertainties provided for the results of the direct method are those arising from the estimated errors in the line intensities. For the results of the P and ONS methods, we have added quadratically the estimated uncertainties of the methods, 0.1 dex, to the uncertainties in the measured line ratios. In the case of the ONS method, the derived uncertainties are in the range 0.10–0.12 dex in all cases, and we decided to adopt an uncertainty of 0.12 dex for this method. For the C method we adopt an uncertainty of 0.10 dex, the value estimated by Pilyugin et al. ([2012](#)) for the case when the line ratios involved in the calculations have uncertainties below 10 per cent. Some of the regions have line ratios with larger uncertainties, up to 40 per cent, but our results below agree with uncertainties around or below 0.10 dex for the oxygen abundances derived with this method in most of the H II regions. We assigned uncertainties of 0.16 and 0.18 dex for the N2 and O3N2 methods, respectively, the ones found in the calibration of these methods, since the errors in the line intensities do not add significantly to this result.

We checked for the effect of the correction for stellar absorption on the oxygen abundances derived for our observed H II regions. The values of $12 + \log(\text{O/H})$ change by 0–0.04 dex in most of our regions for the direct, ONS, C, O3N2, and N2 methods. The exceptions are region 24, where the results of the direct method increase by 0.08 dex with the correction, and region 6, the one with the largest correction, where the oxygen abundance derived with the ONS method increases by 0.13 dex. The results of the P method are more sensitive to this correction, with six regions showing increments larger than 0.10 dex: regions 7, 21, and 44, where the oxygen abundance increases by ~0.15 dex, and regions 6, 14, and 26, with increments of 0.49, 0.28, and 0.24, respectively.

We have calculated the galactocentric distances of the observed H II regions assuming a planar geometry for M81, with a rotation angle of the major axis of M81 of 157°, a disc inclination of 59° (Kong et al. [2000](#)), and a distance of 3.63 ± 0.34 Mpc (Freedman et al. [2001](#)). Our 48 H II regions cover a range of galactocentric distances of 4.8–9.0 kpc. In order to increase this range, we selected from the literature other observations of H II regions in M81. This also allows us to look for observational effects on the derived abundances. The final sample is composed of 116 H II regions spanning a range of galactocentric distances of 3–33 kpc, where 48 H II regions are from this work and the remaining 68 from the works of Garnett & Shields ([1987](#)), Bresolin, Kennicutt & Garnett ([1999](#)), Stanghellini et al. ([2010](#)), and Patterson et al. ([2012](#)). We applied the same procedures explained above to derive physical conditions and oxygen abundances for the H II regions from the literature, using the line intensities reported in the original papers. We also recalculated the galactocentric distances of these H II regions using the same parameters stated above for M81. The results are presented in Tables [5](#) and [6](#).

The direct method could be applied to 31 H II regions of the final sample where the electron temperature can be estimated ($T_e([\text{N II}])$, $T_e([\text{O III}])$, or both): 12 from this work, 13 from Stanghellini et al. ([2010](#)) and six from Patterson et al. ([2012](#)). The strong-line methods were applied to all the regions in the final sample. Fig. [3](#) shows the oxygen abundances obtained with the different methods we are using as a function of galactocentric distance for the H II regions in our final sample. Panel (a) shows the results for the 31

Table 5. Oxygen and nitrogen abundances for the regions observed by Patterson et al. (2012) and Stanghellini et al. (2010).

ID	R (kpc)	T_e([N II])/T_e([O III]) (K)	(T_e)	12 + log (O/H) (P)	(ONS)	(C)	(O3N2)	(N2)	12 + log (N/H) (T_e)	(ONS)	(C)
				Patterson et al. (2012)							
02	22.6	–	–	8.08	8.43	8.53	8.42	8.46	–	7.33	7.40
03	22.2	–	–	8.25	8.43	8.40	8.37	8.46	–	7.41	7.40
07	22.8	–	–	7.78	8.51	8.52	8.54	8.48	–	7.32	7.24
14	14.6	–	–	8.41	8.57	8.44	8.29	8.39	–	7.54	7.45
17	21.6	–	–	8.29	8.39	8.37	8.26	8.27	–	7.07	7.03
21	15.9	$14100 \pm 3800/11200^{+1000}_{-700}$	$8.16^{+0.13}_{-0.10}$	8.27	8.48	8.33	8.20	8.34	$7.41^{+0.17}_{-0.24}$	7.47	7.39
24	16.1	–	–	8.28	8.56	8.43	8.32	8.42	–	7.45	7.36
25	15.0	–	–	8.07	8.49	8.45	8.50	8.52	–	7.40	7.41
26	31.1	–	–	8.33	8.35	8.29	8.23	8.28	–	7.11	7.05
28	31.4	$-/12700^{+900}_{-700}$	$8.19^{+0.06}_{-0.07}$	8.15	8.41	8.24	8.12	8.26	$7.23^{+0.07}_{-0.08}$	7.33	7.24
29	29.2	–	–	7.99	8.24	8.47	8.50	8.36	–	6.93	7.08
33	32.7	–	–	8.23	8.41	8.21	8.24	8.27	–	7.21	6.87
35	24.1	–	–	7.62	8.33	8.28	8.38	8.51	–	7.19	7.17
37	21.9	–	–	8.01	8.40	8.43	8.37	8.44	–	7.26	7.27
Disc1	6.4	$7500^{+900}_{-500}/7300^{+700}_{-400}$	$8.74^{+0.16}_{-0.20}$	8.21	8.45	8.49	8.47	8.56	$7.82^{+0.18}_{-0.22}$	7.61	7.66
Disc2	11.5	–	–	8.16	8.46	8.47	8.48	8.53	–	7.55	7.55
Disc3	10.2	$8500^{+2000}_{-900}/9500^{+1000}_{-600}$	$8.55^{+0.20}_{-0.25}$	8.24	8.42	8.43	8.32	8.48	$7.56^{+0.24}_{-0.30}$	7.49	7.51
Disc4	7.9	$7800^{+900}_{-600}/-$	$8.67^{+0.16}_{-0.19}$	8.29	8.46	8.53	8.46	8.53	$7.78^{+0.18}_{-0.21}$	7.62	7.68
Disc5	5.7	$7900^{+1000}_{-600}/-$	$8.60^{+0.17}_{-0.19}$	8.42	8.48	8.47	8.44	8.53	$7.80^{+0.19}_{-0.22}$	7.71	7.72
Disc6	5.0	–	–	8.39	8.48	8.50	8.46	8.53	–	7.70	7.73
Disc7	2.9	–	–	8.27	8.55	8.57	8.59	8.61	–	7.86	7.88
				Stanghellini et al. (2010)							
HII4	9.3	$10800^{+9200}_{-2300}/-$	$8.12^{+0.40}_{-0.41}$	8.31	8.44	8.46	8.33	8.47	$7.32^{+0.45}_{-0.52}$	7.50	7.53
HII5	8.9	$11100 \pm 300/-$	8.06 ± 0.04	7.95	8.44	8.52	8.49	8.56	7.29 ± 0.04	7.45	7.52
HII21	8.7	–	–	7.63	8.36	8.48	8.46	8.60	–	7.37	7.45
HII31	8.8	$8400^{+10300}_{-1400}/-$	$8.59^{+0.40}_{-0.81}$	7.93	8.46	8.53	8.52	8.56	$7.63^{+0.54}_{-1.02}$	7.46	7.51
HII42	9.0	–	–	7.88	8.41	8.45	8.47	8.57	–	7.41	7.46
HII72	6.9	$10300^{+3400}_{-1400}/-$	$8.12^{+0.21}_{-0.26}$	8.32	8.45	8.47	8.34	8.43	$7.21^{+0.25}_{-0.30}$	7.42	7.43
HII78	9.0	–	–	7.82	8.52	8.53	8.61	8.65	–	7.58	7.62
HII79	8.3	$9200^{+3200}_{-1200}/-$	$8.25^{+0.27}_{-0.42}$	8.30	8.45	8.50	8.38	8.47	$7.32^{+0.31}_{-0.48}$	7.47	7.51
HII81	7.2	$9100^{+10900}_{-1600}/-$	$8.39^{+0.41}_{-0.86}$	8.07	8.41	8.48	8.42	8.52	$7.42^{+0.52}_{-1.11}$	7.42	7.47
HII123	7.9	$8900^{+1000}_{-700}/-$	$8.46^{+0.14}_{-0.17}$	8.14	8.43	8.54	8.42	8.48	$7.45^{+0.16}_{-0.19}$	7.40	7.47
HII133	6.9	$11800^{+400}_{-300}/-$	7.95 ± 0.04	8.22	8.42	8.47	8.38	8.50	7.21 ± 0.04	7.47	7.52
HII201	6.9	$-/13300^{+2400}_{-1300}$	$7.83^{+0.10}_{-0.13}$	8.48	8.51	8.36	8.28	8.40	$7.18^{+0.12}_{-0.14}$	7.60	7.50
HII213	9.7	–	–	7.76	8.39	8.50	8.46	8.56	–	7.35	7.42
HII228	10.1	$9300 \pm 300/-$	8.36 ± 0.06	8.01	8.46	8.50	8.49	8.53	$7.44^{+0.06}_{-0.07}$	7.44	7.47
HII233	5.9	–	–	8.02	8.48	8.53	8.53	8.58	–	7.55	7.61
HII249	10.6	–	–	7.49	8.34	8.48	8.44	8.57	–	7.27	7.34
HII262	9.9	$11500^{+1100}_{-800}/-$	$8.19^{+0.11}_{-0.13}$	7.69	8.36	8.45	8.44	8.57	$7.31^{+0.12}_{-0.14}$	7.32	7.40
HII282	5.1	–	–	8.09	8.48	8.52	8.52	8.55	–	7.54	7.57
HII325	9.5	$10800 \pm 2500/-$	$8.14^{+0.46}_{-0.23}$	8.15	8.41	8.45	8.37	8.47	$7.22^{+0.47}_{-0.36}$	7.36	7.40
HII352	10.7	–	–	7.24	8.26	8.37	8.38	8.61	–	7.25	7.32
HII384	7.0	–	–	8.14	8.49	8.51	8.52	8.54	–	7.56	7.59
HII403	9.9	$9400^{+2400}_{-1100}/-$	$8.57^{+0.23}_{-0.31}$	7.74	8.35	8.44	8.41	8.54	$7.49^{+0.26}_{-0.35}$	7.27	7.34

H II regions with some temperature estimate that allows us to use the direct method; panels (b) to (f) show the results obtained with the strong-line methods for the 116 H II regions of the whole sample. In panel (b) we plot with open symbols the results for the 14 regions that are classified as belonging to the upper branch of the metallicity relation, but whose values of 12 + log (O/H), derived with this relation, fall below 8.0, the region of the lower branch.

We fitted straight lines with the least-squares method to the data in Fig. 3 in order to derive the abundance gradient implied by each of the methods used for the abundance determination. Weighted least-squares fits produce similar values for the parameters, but we present the non-weighted results because some of the data seem to be affected by systematic errors, and we do not think that a robust estimation is required for our purposes. The fits are plotted in Fig. 3, and the parameters of the fitted gradients are listed in Table 7, where we list for each method the number of regions used (*N*), the intercept and the slope of the fit, and the standard deviation of the points from this fit. In the case of the P method, we excluded from the fit the regions where this method does not seem to be working properly (see above). The discontinuous line in panel (b) shows the results when these regions are included. The intercept and slope for this fit are 8.48 ± 0.03 and -0.018 ± 0.004, respectively, with a dispersion of 0.24 dex.

Table 6. Oxygen and nitrogen abundances for the regions observed by Bresolin et al. (1999) and Garnett & Shields (1987).

ID	R		12 + log (O/H)				12 + log (N/H)	
	(kpc)	(P)	(ONS)	(C)	(O3N2)	(N2)	(ONS)	(C)
			Bresolin et al. (1999)					
GS1	5.5	8.35	8.48	8.53	8.45	8.50	7.60	7.64
GS2	4.8	8.35	8.47	8.51	8.43	8.50	7.57	7.59
GS4	8.6	8.24	8.43	8.49	8.34	8.46	7.41	7.45
GS7	9.0	8.18	8.44	8.49	8.46	8.54	7.52	7.56
GS9	6.5	8.40	8.49	8.50	8.49	8.57	7.77	7.79
GS11	5.6	8.51	8.50	8.49	8.41	8.52	7.75	7.75
GS12	5.0	8.14	8.47	8.54	8.49	8.52	7.50	7.54
GS13	4.8	8.52	8.57	8.58	8.54	8.54	7.92	7.93
Münch1	16.0	8.13	8.47	8.29	8.16	8.33	7.43	7.34
Münch18	10.1	8.48	8.56	8.37	8.28	8.42	7.73	7.62
			Garnett & Shields (1987)					
HK105	9.2	7.99	8.48	8.44	8.50	8.50	7.39	7.36
HK152	5.6	8.41	8.51	8.49	8.46	8.48	7.63	7.62
HK230	4.8	8.58	8.57	8.47	8.51	8.55	7.98	7.94
HK268	5.5	8.48	8.51	8.53	8.45	8.51	7.72	7.75
HK305-12	5.1	8.48	8.50	8.49	8.41	8.51	7.73	7.73
HK343-50	4.8	8.40	8.48	8.47	8.43	8.50	7.63	7.63
HK453	5.0	8.21	8.48	8.47	8.49	8.52	7.54	7.54
HK472	4.0	8.39	8.53	8.47	8.56	8.60	7.94	7.88
HK500	5.6	8.57	8.54	8.39	8.35	8.49	7.82	7.78
HK652	6.5	8.47	8.51	8.45	8.48	8.56	7.82	7.81
HK666	7.0	8.37	8.46	8.42	8.37	8.50	7.62	7.59
HK712	7.0	8.54	8.50	8.38	8.31	8.42	7.64	7.57
HK741	9.0	8.29	8.47	8.49	8.45	8.53	7.54	7.56
HK767	8.6	8.30	8.44	8.49	8.35	8.48	7.47	7.54
Münch18	10.1	8.47	8.51	8.36	8.31	8.50	7.85	7.78

4.2 Nitrogen abundances and the N/O abundance gradient

The N/H and N/O abundance ratios were calculated using the direct method for 31 H II regions and the ONS and C methods for the whole sample. Tables 5, 6, and 8 show the results.

Fig. 4 shows the results for the N/H and N/O abundances as a function of galactocentric distance. Panels (a) and (c) are for the abundances obtained with the direct method and panels (b) and (d) those for the ONS method. For ease of comparison, the panels cover the same range in orders of magnitude that we used in Fig. 3. We have not plotted the results of the C method, because they show a similar distribution of values to those of the ONS method. The least-squares fits to the data are also plotted in the figure, and in Table 9 we list for each method the number of regions used in the fits, the derived intercepts and slopes, and the dispersions around the gradients. The slopes obtained with the ONS and C methods are very similar, ~ -0.020 dex kpc^{-1}, whereas the direct method implies a shallower slope, -0.008 dex kpc^{-1}. The N/H abundance ratios derived with the ONS and C methods can be assigned uncertainties of ~ 0.10–0.15 dex. The methods do not provide estimates of the uncertainties in the derived N/O abundance ratios, but the dispersions around the gradients implied by these methods suggest that the random uncertainties are ~ 0.1 dex.

4.3 Comparison with other works

The values that we obtain for the slope of the metallicity gradient go from -0.010 to -0.002 dex kpc^{-1}, smaller in absolute values than most other determinations of the oxygen abundance gradient in M81. Table 10 provides a compilation of some previous results

ordered chronologically, where we list the method and number of regions used in each case, the range of galactocentric distances covered by the objects and the intercept and the slope of the fits. Besides two old determinations based on the R$_{23}$ method calibrated with photoionization models by Pagel et al. (1979), we have chosen to present the results that are based on methods similar to the ones we use. The most recent determination, that of Pilyugin et al. (2014), is based on abundances calculated with the P and C methods slightly modified, which we label as P' and C'. Pilyugin et al. (2014) also derived the gradient for N/H with their C' method for regions with galactocentric distances in the range 4–13 kpc, finding a slope of -0.033, steeper than the one we find with the C method for the range of 3–33 kpc, -0.020.

The results shown in Figs 3 and 4, and Tables 7, 9, and 10 illustrate the well-known fact that gradient determinations are very sensitive to the method, to the number of objects used, and to the range of galactocentric distances covered by these objects.

Our results with the P method are very similar to those obtained by Patterson et al. (2012) with this method, and this is the case where both the procedure followed in the abundance determination and the range of galactocentric distances covered agree more closely. Patterson et al. (2012) use larger error bars than we do for the results of the P method and do a weighted least-squares fit, but the main difference between their results and ours is in the abundances obtained for the H II regions observed by Stanghellini et al. (2010), which they also use. The oxygen abundances that we derive for these regions are lower than the ones they find. This is clearly seen in panel (b) of Fig. 3 where several objects located between 8 and 11 kpc have oxygen abundances much lower than 12 + log (O/H) = 8.0, whereas Patterson et al. (2012) find 12 + log (O/H) > 8.0
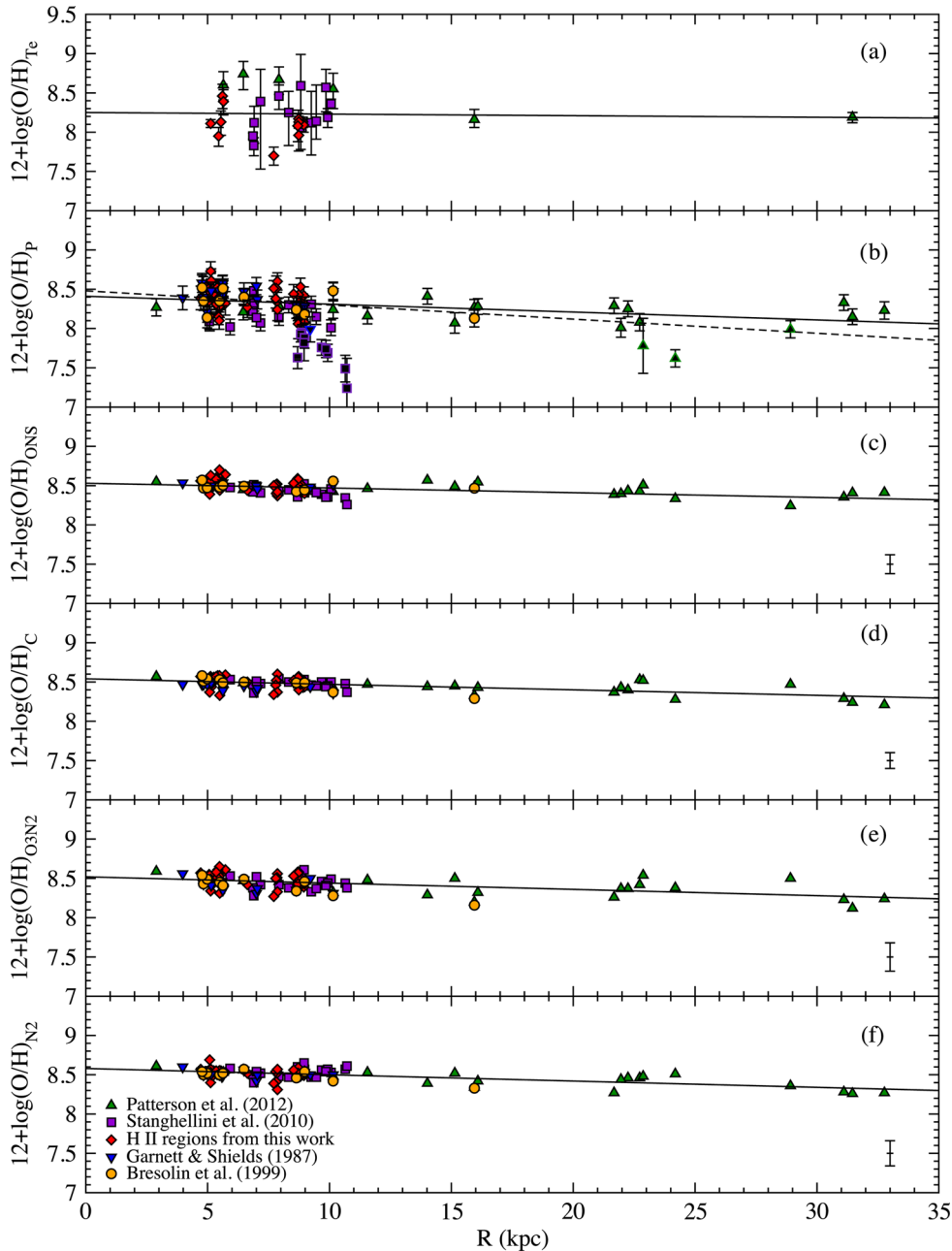
Figure 3. Oxygen abundances in H II regions of M81 as a function of their galactocentric distances and the abundance gradients resulting from our fits. Panels (a) to (f) show the results of the direct method and the methods P, ONS, C, O3N2, and N2. The different symbols indicate the references for the observational data we used, and are identified in panel (f). Panels (c) to (f) show in the lower right corner the typical uncertainty in the oxygen abundances derived with the corresponding method. In panel (b) we also plot with a discontinuous line the gradient fitted when the regions where the P method is not working (plotted as empty symbols; see text) are included in the fit. Note that all the panels are at the same scale.

for all these regions. These differences are partly due to the fact that Patterson et al. (2012) do not include all the H II regions of Stanghellini et al. (2010), but use only those for which there is also an estimate of the electron temperature. However, we can only reproduce their results for the H II regions in common if we use the line ratios of Stanghellini et al. (2010) uncorrected for extinction, which Patterson et al. (2012) seem to have inadvertently done. The results we derive with the P method for the H II regions observed by Patterson et al. (2012) agree within 0.01 dex with the ones derived by these authors with the exception of four objects which belong to the upper branch of the metallicity calibration according to our

classification scheme (see Section 3.2.1), but are in an ambiguous region according to the procedure followed by Patterson et al. (2012). For these regions they calculate an average of the oxygen abundances implied by the upper and lower branch of the calibration, obtaining values that differ from the ones we calculated, using their line intensities, by 0.05–0.26 dex.

On the other hand, there are several H II regions in our full sample which are classified as belonging to the upper branch following both our classification scheme and the one used by Patterson et al. (2012), but whose abundances, calculated using the upper-branch relation of the P method, lie in the region that should be covered by the lower

Table 7. Oxygen abundance gradients and dispersions.

Method	N	$12 + \log(O/H)_0$	$\frac{\Delta(\log(O/H))}{\Delta(R)}$ (dex kpc^{-1})	σ
T_e	31	8.26 ± 0.10	-0.002 ± 0.010	0.25
P	102	8.41 ± 0.03	-0.010 ± 0.003	0.15
ONS	116	8.53 ± 0.01	-0.006 ± 0.001	0.07
C	116	8.54 ± 0.01	-0.007 ± 0.001	0.06
O3N2	116	8.52 ± 0.02	-0.008 ± 0.001	0.09
N2	116	8.58 ± 0.01	-0.008 ± 0.001	0.06

branch [all the regions with $12 + \log(O/H) \leq 8.0$ in Fig. 3(b), which are plotted as empty symbols, and in the lower panel of fig. 10 of Patterson et al. 2012]. Our observed regions do not show this problem, but two of them, regions 14 and 44, would have the same behaviour if we had not corrected their spectra for the effects of stellar absorption: the uncorrected spectra imply values of $12 + \log(O/H) = 7.76$ and 8.00, whereas the corrected spectra change those values to 8.06 and 8.16, respectively. Since neither Patterson et al. (2012) nor Stanghellini et al. (2010) correct their spectra for stellar absorption, the regions they observed where the P method has problems might also be affected in the same way. We do not

Table 8. The nitrogen abundances derived with the direct method (T_e) and two strong-line methods (ONS and C) for the 48 regions in our observed sample.

| ID	$12 + \log(N/H)$			$\log(N/O)$		
	(T_e)	(ONS)	(C)	(T_e)	(ONS)	(C)
1	$7.39^{+0.08}_{-0.09}$	7.58	7.58	-0.76 ± 0.05	-0.87	-0.85
2	$7.35^{+0.10}_{-0.12}$	7.53	7.59	-0.75 ± 0.06	-0.91	-0.93
3	–	7.61	7.62	–	-0.87	-0.87
4	–	7.46	7.50	–	-0.94	-0.94
5	$7.34^{+0.18}_{-0.23}$	7.62	7.69	$-0.63^{+0.10}_{-0.09}$	-0.84	-0.86
6	–	7.70	7.65	–	-0.83	-0.82
7	–	7.54	7.56	–	-0.92	-0.93
8	$7.50^{+0.13}_{-0.14}$	7.68	7.68	$-0.68^{+0.07}_{-0.06}$	-0.81	-0.78
9	–	7.73	7.72	–	-0.84	-0.85
10	$7.48^{+0.09}_{-0.10}$	7.65	7.64	-0.65 ± 0.06	-0.79	-0.76
11	–	7.70	7.72	–	-0.80	-0.78
12	$7.34^{+0.19}_{-0.24}$	7.53	7.59	$-0.74^{+0.11}_{-0.09}$	-0.90	-0.92
13	–	7.65	7.64	–	-0.94	-0.92
14	–	7.61	7.63	–	-0.90	-0.90
15	–	7.68	7.67	–	-0.91	-0.89
16	–	7.85	7.85	–	-0.68	-0.67
17	$7.14^{+0.13}_{-0.15}$	7.65	7.56	-0.56 ± 0.08	-0.85	-0.78
18	–	7.55	7.59	–	-0.89	-0.91
19	–	7.58	7.71	–	-0.79	-0.89
20	–	7.66	7.67	–	-0.86	-0.85
21	–	7.48	7.62	–	-0.91	-0.90
22	–	7.73	7.71	–	-0.78	-0.75
23	–	7.71	7.70	–	-0.71	-0.67
24	$7.35^{+0.14}_{-0.17}$	7.60	7.61	-0.68 ± 0.07	-0.98	-0.93
25	–	7.52	7.53	–	-0.98	-1.00
26	–	7.74	7.64	–	-0.96	-0.94
27	–	7.99	7.95	–	-0.56	-0.52
28	–	7.89	7.84	–	-0.68	-0.63
29	–	8.16	8.07	–	-0.48	-0.42
30	–	7.68	7.72	–	-0.82	-0.83
31	–	7.76	7.73	–	-0.86	-0.85
32	–	7.74	7.73	–	-0.70	-0.60
33	$7.52^{+0.16}_{-0.21}$	7.76	7.77	-0.62 ± 0.09	-0.79	-0.79
34	–	7.80	7.79	–	-0.73	-0.71
35	$7.73^{+0.17}_{-0.19}$	7.79	7.75	$-0.75^{+0.09}_{-0.08}$	-0.74	-0.74
36	$7.69^{+0.18}_{-0.21}$	7.76	7.75	-0.71 ± 0.10	-0.75	-0.74
37	–	7.81	7.78	–	-0.83	-0.81
38	–	7.79	7.81	–	-0.75	-0.74
39	–	7.86	7.87	–	-0.69	-0.69
40	$7.47^{+0.06}_{-0.07}$	7.71	7.69	-0.65 ± 0.04	-0.81	-0.79
41	–	7.77	7.76	–	-0.72	-0.68
42	–	7.88	7.88	–	-0.70	-0.68
43	–	7.89	7.74	–	-0.73	-0.83
44	–	7.78	7.82	–	-0.60	-0.55
45	–	7.83	7.81	–	-0.75	-0.74
46	–	7.78	7.78	–	-0.80	-0.79
47	–	7.79	7.81	–	-0.74	-0.72
48	–	7.85	7.87	–	-0.71	-0.70
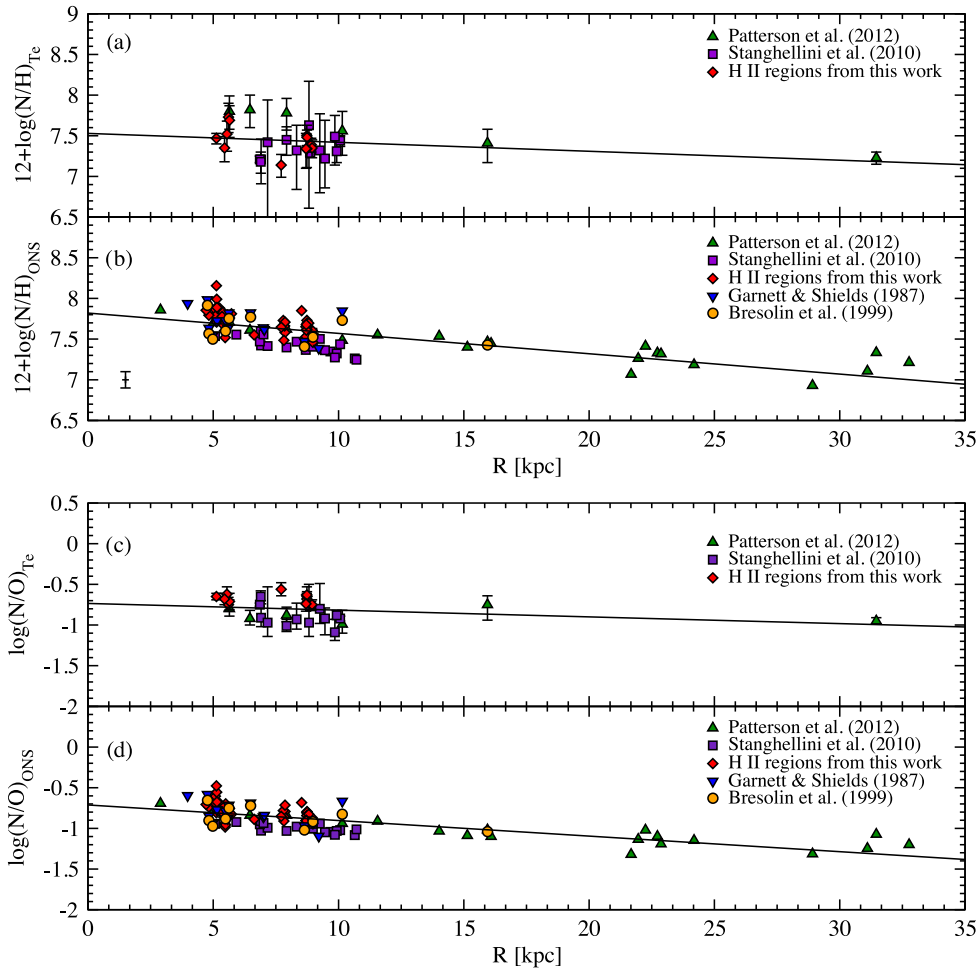
Figure 4. N/H and N/O abundances in the H II regions of M81 as a function of their galactocentric distances and the abundance gradients resulting from the fits. Panels (a) and (c) show the results of the direct method, and panels (b) and (d) the results of the ONS method. The different symbols indicate the references for the observational data we used. In all panels, the vertical scale spans the same range in orders of magnitude displayed in Fig. 3.

Table 9. N/H and N/O abundance gradients and dispersions.

Method	N	$12 + \log(N/H)_0$	$\frac{\Delta(\log(N/H))}{\Delta(R)}$ (dex kpc^{-1})	σ	$\log(N/O)_0$	$\frac{\Delta(\log(N/O))}{\Delta(R)}$ (dex kpc^{-1})	σ
T_e	31	7.53 ± 0.07	-0.011 ± 0.007	0.18	-0.73 ± 0.05	-0.008 ± 0.005	0.13
ONS	116	7.82 ± 0.03	-0.025 ± 0.002	0.15	-0.71 ± 0.05	-0.019 ± 0.002	0.11
C	116	7.85 ± 0.02	-0.020 ± 0.002	0.12	-0.69 ± 0.05	-0.020 ± 0.002	0.13

consider in our fit of Table 7 the H II regions where the P method is not working properly. If we include them, we get an intercept and slope for the gradient of 8.48 ± 0.03 and -0.018 ± 0.004, respectively, with a dispersion of 0.24 dex. This fit is plotted with a discontinuous line in Fig. 3(b). Patterson et al. (2012) did not reject from their fits the objects that had problems with the P method, and the gradients they derive with this method are intermediate between our two fits.

Our results for the abundances implied by the direct method in the H II regions observed by Stanghellini et al. (2010) are significantly different from those derived by these authors: we get oxygen abundances that are lower by up to 0.3 dex. The differences are mainly due to the fact that Stanghellini et al. (2010) calculated the neutral oxygen abundance in several objects using [O I] emission and added it to the O^+ and O^{++} abundances to get the total oxy-

gen abundance as can be seen in their table 3, available online; see, for example, the results for their region number 5. This is not a procedure usually followed for H II regions since the ionization potentials of O^0 and H^0 are both $\simeq 13.6$ eV, suggesting that [O I] emission should arise in regions close to the ionization front. Besides, charge-exchange reactions between O^0 and H^+ tend to keep O^0 outside the ionized region (Osterbrock & Ferland 2006). The O^0/H^+ abundance ratios derived by Stanghellini et al. (2010) are also very high, 30 to 230 times larger than the ones we estimate. Since Patterson et al. (2012) compared their results with the direct method with those reported by Stanghellini et al. (2010), they found a better agreement of the two sets than the one that can be observed in Fig. 3.

The differences between the abundances we derive with the direct method using the line intensities of Patterson et al. (2012) and the

Table 10. Oxygen abundance gradients from the literature.

Method	N	ΔR (kpc)	$\log(O/H)_0$ +12	$\frac{\Delta(\log(O/H))}{\Delta(R)}$ (dex kpc^{-1})	Ref.
R_{23}	10	4–8	–	-0.045	1
R_{23}	18	3–15	–	-0.08	2
P	36	4–12	8.69	-0.031	3
T_e	31	4–17	9.37 ± 0.24	-0.093 ± 0.020	4
P	21	3–33	8.34 ± 0.12	-0.013 ± 0.006	5
P	49	3–33	8.47 ± 0.06	-0.016 ± 0.006	5
T_e	7	6–32	8.76 ± 0.13	-0.020 ± 0.006	5
T_e	28	5–10	9.20 ± 0.11	-0.088 ± 0.013	6
$P'+C'$	–	4–13	8.58 ± 0.02	-0.011 ± 0.003	7

Notes. References: (1) Stauffer & Bothun (1984), (2) Garnett & Shields (1987), (3) Pilyugin et al. (2004), (4) Stanghellini et al. (2010), (5) Patterson et al. (2012), (6) Stanghellini et al. (2014), (7) Pilyugin et al. (2014).

values given by these authors are below 0.2 dex, and seem to be due to typos in their tables. For example, Patterson et al. (2012) give a value for T_e([O III]) for their region 26, but no intensity is provided for the [O III] $\lambda4363$ line for this region in their table 2. In addition, some of the values they list for the total oxygen abundance in their table 4, and plot in their figures, are transposed, namely the values of O/H given for their regions disc1, disc3, and disc4. If we add the values of O$^+$/H$^+$ and O^{++}/H$^+$ listed in their table 4 for each of these regions, we get the total oxygen abundance that they attribute to a different region; for example, the oxygen abundance implied by their ionic abundances in disc3 is assigned by them to region disc4. These differences, along with the fact that our observations lead to lower oxygen abundances for the galactocentric range in common with the other samples, explain the very different value that we obtain with the direct method for the abundance gradient, -0.002 dex kpc^{-1} versus -0.020 dex kpc^{-1} (the result of Patterson et al. 2012, that covers a range of galactocentric distances similar

to ours). An inspection of Fig. 3(a) shows that the inclusion of data from different works is the main reason of this difference: we would get a steeper gradient if we only used the data obtained by Patterson et al. (2012).

We have several regions in common with other authors, and Table 11 shows a comparison between the oxygen and nitrogen abundances we derive with different methods using the line intensities reported for each region. The apertures are different, and in two cases we extracted the spectra of two knots at the positions covered by other works, but the differences in the abundances implied by each method are of the same order as the differences that we find in Figs 3 and 4 for regions at similar galactocentric distances. Since these differences depend on the method and in some cases are larger than the estimated uncertainties, we think that the results in Table 11 and Figs 3 and 4 illustrate the robustness of the methods to different observational problems that are not necessarily included in the estimates of the uncertainties in the line intensities. The data obtained by different authors will be affected in different amounts by uncertainties that are difficult to estimate, such as those introduced by atmospheric differential refraction (Filippenko 1982), flux calibration or extraction, extinction correction, and the measurement of weak lines in spectra that are not deep enough or have poor spectral resolution. Those methods that give consistent results when applied to different sets of observations can be considered more robust to these observational effects.

5 DISCUSSION

The question of whether a single straight-line fit describes well the metallicity gradient in a galaxy is often raised (see e.g. Patterson et al. 2012). This does not concern us here. We have fitted straight lines in order to see the dependence of the slope on the method used for the abundance determination and to measure the dispersion of the results around these fits. We would get similar dispersions if

Table 11. Comparison of our results for the H II regions in common with other samples.

ID	Ref.	T_e([N II]) (K)	(T_e)	12 + log (O/H) (P)	(ONS)	(C)	(O3N2)	(N2)	12 + log (N/H) (T_e)	(ONS)	(C)
1	1	10100^{+500}_{-400}	$8.13^{+0.06}_{-0.07}$	8.33	8.45	8.43	8.42	8.53	$7.39^{+0.08}_{-0.09}$	7.58	7.58
HII31	2	8400^{+10300}_{-1400}	$8.59^{+0.40}_{-0.81}$	7.93	8.46	8.53	8.52	8.56	$7.63^{+0.54}_{-1.02}$	7.46	7.51
GS7	3	–	–	8.18	8.44	8.49	8.46	8.54	–	7.52	7.56
HK741	4	–	–	8.29	8.47	8.49	8.45	8.53	–	7.54	7.56
15	1	–	–	8.28	8.58	8.56	8.57	8.52	–	7.68	7.67
GS4	3	–	–	8.24	8.43	8.49	8.34	8.46	–	7.41	7.45
HK767	4	–	–	8.30	8.44	8.49	8.35	8.48	–	7.47	7.54
35	1	8200^{+700}_{-600}	$8.46^{+0.15}_{-0.16}$	8.57	8.53	8.49	8.39	8.49	$7.73^{+0.17}_{-0.19}$	7.79	7.75
Disc5	5	7900^{+1000}_{-600}	$8.60^{+0.17}_{-0.19}$	8.42	8.48	8.47	8.44	8.53	$7.80^{+0.19}_{-0.22}$	7.71	7.72
GS11	3	–	–	8.51	8.50	8.49	8.41	8.52	–	7.75	7.75
HK500	4	–	–	8.57	8.54	8.39	8.35	8.49	–	7.82	7.78
38	1	–	–	8.35	8.54	8.55	8.55	8.56	–	7.79	7.81
39	1	–	–	8.47	8.56	8.56	8.54	8.55	–	7.86	7.87
GS12	3	–	–	8.14	8.47	8.54	8.49	8.52	–	7.50	7.54
HK453	4	–	–	8.21	8.48	8.47	8.49	8.52	–	7.54	7.54
Disc6	5	–	–	8.39	8.48	8.50	8.46	8.53	–	7.70	7.73
47	1	–	–	8.56	8.53	8.53	8.44	8.51	–	7.79	7.81
48	1	–	–	8.39	8.56	8.57	8.57	8.57	–	7.85	7.87
GS13	3	–	–	8.52	8.57	8.58	8.54	8.54	–	7.92	7.93
HK230	4	–	–	8.58	8.57	8.47	8.51	8.55	–	7.98	7.94

References for the ID and line intensities: (1) this work, (2) Stanghellini et al. (2010), (3) Bresolin et al. (1999), (4) Garnett & Shields (1987), (5) Patterson et al. (2012).
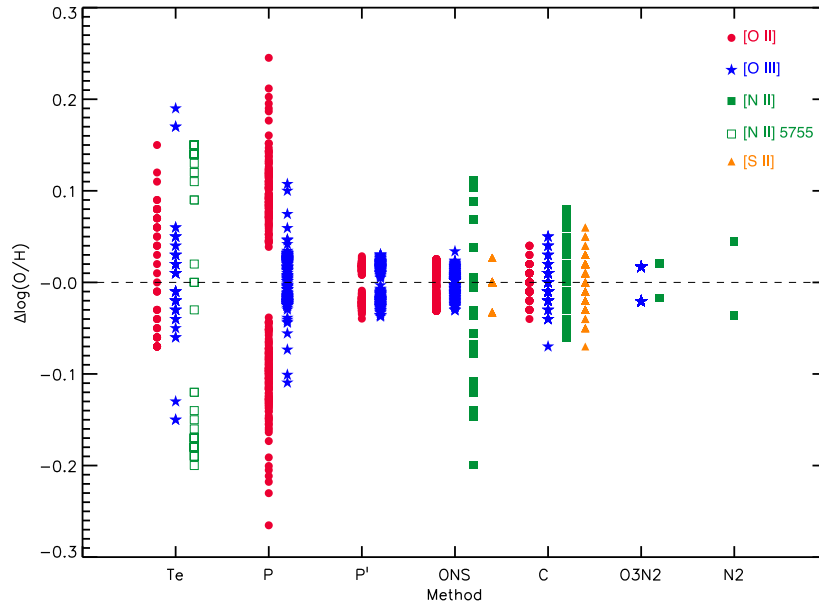
Figure 5. Changes in the oxygen abundances for our sample of H II regions introduced by changes of 20 per cent in the main line ratios used by each method. Circles, stars, squares and triangles are used to represent changes in line ratios involving lines of [O II], [O III], [N II], and [S II], respectively. '[N II] 5755' implies changes in the [N II] ($\lambda6548 + \lambda6583$)/$\lambda5755$ intensity ratio, '[N II]' implies changes in the [N II] ($\lambda6548 + \lambda6583$)/H$\beta$ ratio for the ONS method, and the [N II] $\lambda6583$/Hβ ratio for the C, O3N2, and N2 methods.

we just measured the dispersion in abundances for regions located at similar galactocentric distances. Besides, the low dispersions around the gradient shown by the abundances derived with the ONS, C, and N2 methods suggest that straight-line fits are good first approximations to the data.

The main objective of this work is to study the effectiveness of the methods in producing robust measurements of abundance variations across a galaxy. One assumption we make is that the more robust methods will produce lower dispersions around the gradient. In the presence of azimuthal variations, we do not expect that any method will imply a dispersion lower than the real one. We think that this is a reasonable assumption. Hence, we use the dispersions introduced by the different methods as a measure of their robustness or sensitivity to the observational data set used. Note that the robustness of a method should not be confused with its reliability. The more robust methods will not necessarily provide better results. The reliability of the direct method depends on the validity of its assumptions; the reliability of the strong-line methods depends on their calibration and on their application to objects that are well represented in the calibration samples. In what follows, we will centre our discussion in the robustness of the methods, and will assume that if a strong-line method does not provide a good estimate of the oxygen abundance, it is possible that it can be better calibrated to do so.

Figs 5 and 6 illustrate the sensitivity of each method to the main line ratios involved in the calculations. We plot in these figures the changes in the O/H, N/H, and N/O abundance ratios resulting from changes of 20 per cent in the main line intensity ratios involved in the calculations for all the regions in our sample. Note that in these figures '[N II] $\lambda5755$' identifies the results of changes in the [N II] ($\lambda6548 + \lambda6583$)/$\lambda5755$ temperature diagnostic, '[N II]' identifies the results of changes in the [N II] ($\lambda6548 + \lambda6583$)/H$\beta$ ratio for the ONS method and the direct method, and the [N II] $\lambda6583$/Hβ ratio for the C, O3N2 and N2 methods.

As expected, the results of the direct method are very sensitive to variations in the line ratio used to derive the electron tempera-

ture. This makes this method vulnerable to different observational problems, especially the ones arising from the measurement of the intensity of the weak line [N II] $\lambda5755$. The P method of Pilyugin & Thuan (2005) shows an even larger sensitivity to changes in the line ratio [O II] $\lambda3727$/Hβ, making it vulnerable to problems introduced by atmospheric differential refraction and defective flux calibrations or extinction corrections. This is even more clear if we consider the dispersion from the gradient implied by this method when the regions where it has problems are included in the fit, 0.24 dex. It can be argued that these two line ratios, [N II] ($\lambda6548 + \lambda6583$)/$\lambda5755$ and [O II] $\lambda3727$/Hβ, are the ones most likely to be affected by observational problems, making the direct method and the P method the least robust methods, in agreement with our results. In fact, the dispersions around the gradients listed in Tables 7 and 9 can be qualitatively understood in terms of the sensitivity of the methods to changes in these two line ratios, shown in Figs 5 and 6.

The results we obtain for N/O with the direct method, shown in Fig. 4(c), can be used to illustrate this effect, since the N/O abundances derived with this method depend mainly on the value of T_e implied by the [N II] ($\lambda6548 + \lambda6583$)/$\lambda5755$ intensity ratio and on the [N II] ($\lambda6548 + \lambda6583$)/[O II] $\lambda3727$ intensity ratio. Our observed regions (the diamonds in this figure) have larger N/O ratios than most of the regions observed by Patterson et al. (2012) and Stanghellini et al. (2010). The values we find for T_e([N II]) in our observed regions are generally higher than those we find for the regions of Patterson et al. (2012) by an amount that can explain the differences in this abundance ratio. On the other hand, we find similar values of T_e([N II]) for our regions and the regions observed by Stanghellini et al. (2010). In this case the differences can be attributed to the large values of the [O II] $\lambda3727$/Hβ measured by Stanghellini et al. (2010) in several regions, which are higher than the ones observed by us and by Patterson et al. (2012). If we compare the values of this line ratio for the regions that have temperature determinations and are located at galactocentric distances between 4 and 11 kpc, we find a range of values 149–338 for our observed objects and 229–327 for the regions observed by Patterson et al.
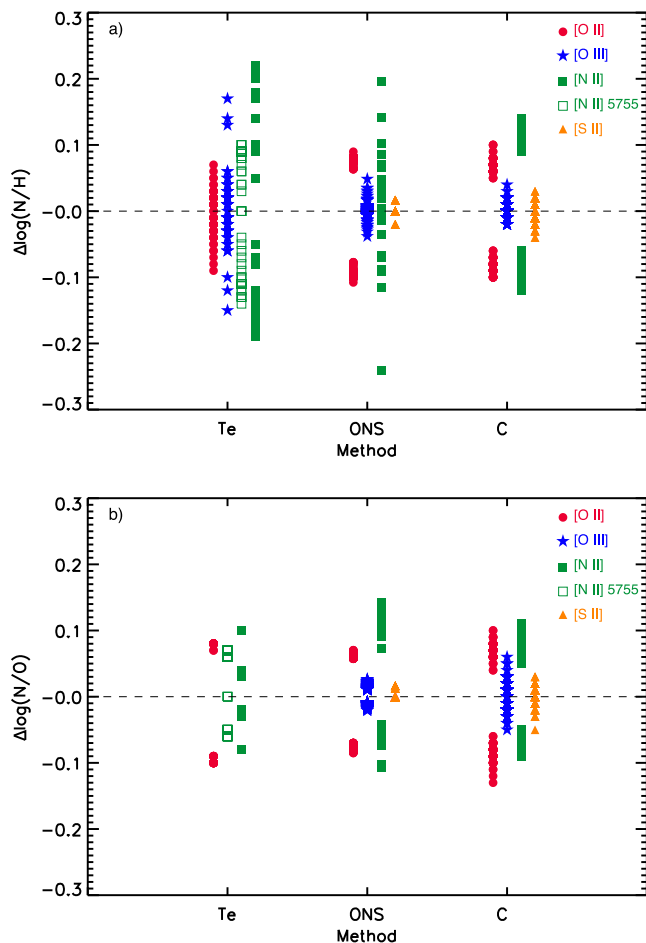
Figure 6. Changes in the N/H and N/O abundance ratios for our sample of H II regions introduced by changes of 20 per cent in the main line ratios used by each method. Circles, stars, squares and triangles are used to represent changes in line ratios involving lines of [O II], [O III], [N II], and [S II], respectively. '[N II] 5755' implies changes in the [N II] ($\lambda6548 + \lambda6583$)/$\lambda5755$ ratio for the direct method, '[N II]' implies changes in the [N II] ($\lambda6548 + \lambda6583$)/H$\beta$ ratio for the direct method and the ONS method, and the [N II] $\lambda6583$/Hβ ratio for the C method.

(2012), whereas the regions observed by Stanghellini et al. (2010) span a range of 180–660. This translates into an [N II] to [O II] line intensity ratio of 0.30–0.59 (this work), 0.15–0.45 (Patterson et al. 2012), and 0.16–0.29 (Stanghellini et al. 2010). The high values of c(Hβ) found by Stanghellini et al. (2010) contribute in part to these differences, but they are already present in their observed intensities.

Any work whose objective is the determination of abundances in H II regions considers an achievement the detection of the weak lines required for the calculation of electron temperature, since temperature-based abundances are expected to be more reliable than those based on strong-line methods. Our results in Fig. 3 and Tables 7 and 11 suggest otherwise. The abundances derived with the direct method are very sensitive to the assumed temperature, which in turn is sensitive to the line intensity ratio used for the diagnostic, as illustrated in Fig. 5. The precision required to get a good estimate of this ratio is often underestimated.

The P method, based on the intensities of strong [O II] and [O III] lines relative to Hβ, seems to be working slightly better in many cases, although there are regions whose abundances show large deviations from their expected values. The results shown in Fig. 5

suggest that the spectra of these regions might have problems related with atmospheric differential refraction, flux calibration or extinction correction. In this context, it would be useful to check whether the deviations are correlated with the airmass during the observation, but none of the papers whose spectra we use provides the airmass values of their observations. The new calibration of the P method of Pilyugin et al. (2014), which we have called P′ above, is less sensitive to the [O II] $\lambda3727$/Hβ line ratio and performs much better when used to derive the oxygen abundance gradient, implying a slope of -0.008 dex kpc^{-1} and a dispersion around the gradient of 0.09 dex. However, the calibration sample of the P′ method includes regions with abundances determined using the C method. Since we have centred here on methods calibrated with H II regions that have temperature measurements, we only show the results of the P method in Fig. 3 and Table 7.

The other strong-line methods, especially the ONS, C, and N2 methods, seem to be working remarkably well (see the dispersions in Table 7 and Fig. 3). These methods suggest that azimuthal variations, if present, are very small. The low dispersion implied by the N2 method is especially remarkable, since it is due to a low dispersion in the values of the [N II] $\lambda\lambda6548, 6583$/Hα intensity ratio that can only arise if N/H and the degree of ionization are both varying smoothly across the disc of M81. Since these quantities and N/O might show different variations in other environments, the N2 method will not necessarily give consistent results for O/H when applied to H II regions in other galaxies or to regions located near galactic centres. In fact, Pérez-Montero & Contini (2009) find that the N2 method can lead to values of O/H that differ from the ones derived with the direct method by up to an order of magnitude. The ONS and C methods should be preferred for this reason, although we note that any strong-line method could easily fail for H II regions whose properties are not represented in the calibration sample (Stasińska 2010). The best estimates of the chemical abundances in H II regions implied by forbidden lines will still be based on the measurement of electron temperatures, but we stress that they require data of high quality.

This is illustrated by the work of Bresolin (2011), who found that the scatter in the oxygen abundances derived with the direct method in the central part of the galaxy M33 is around 0.06 dex when using his observations, whereas the data of Rosolowsky & Simon (2008) lead to much larger variations, with a dispersion of 0.21 dex. The spectra of Bresolin (2011) were deeper than the ones observed by Rosolowsky & Simon (2008), which might explain this result, although there could be other effects involved in the explanation. Another example of the low dispersion that can be found with the direct method is provided by Bresolin et al. (2009) for NGC 300, where 28 H II regions covering a relatively large range of galactocentric distances show a dispersion around the gradient of only 0.05 dex.

6 SUMMARY AND CONCLUSIONS

We have used long slit spectra obtained with the GTC telescope to extract spectra for 48 H II regions in the galaxy M81. We have added to this sample the spectra of 68 H II regions in M81 observed by different authors (Garnett & Shields 1987; Bresolin et al. 1999; Stanghellini et al. 2010; Patterson et al. 2012). This sample was re-analysed using the line intensities reported in each work. We followed the same procedure that we applied in our sample to calculate physical properties, chemical abundances and galactocentric distances for these H II regions. The final sample contains 116 H II regions that cover a range of galactocentric distances of 3–33 kpc.

We have used these data to derive the oxygen and nitrogen abundance gradients in M81. We could calculate the electron temperature and apply the direct method to 31 H II regions of the sample. We used different strong-line methods to derive oxygen and nitrogen abundances for the full sample. We have chosen strong-line methods calibrated with large samples of H II regions with temperature-based abundance determinations: the P method of Pilyugin & Thuan ([2005](#)), the ONS method of Pilyugin et al. ([2010](#)), the C method of Pilyugin et al. ([2012](#)), and the O3N2 and N2 methods calibrated by Marino et al. ([2013](#)).

We have fitted straight lines to the variation with galactocentric distance of the oxygen abundances implied by each method. We find metallicity gradients with slopes that go from -0.010 to -0.002 dex kpc^{-1}. The two extreme values are derived with the P method and the direct method (the shallower value). These two methods are the ones that are more sensitive to variations in two of the line ratios, most likely affected by observational problems, [N II] $(\lambda 6548 + \lambda 6583)/\lambda 5755$ and [O II] $\lambda 3727/$Hβ, and show the largest dispersions around the gradient, 0.25 and 0.15 dex, respectively, whereas the ONS, C, O3N2, and N2 methods imply oxygen abundance gradients in the range from -0.008 to -0.006 dex kpc^{-1} and very low dispersions, equal to 0.06 dex, for the C and N2 methods, 0.07 dex for the ONS method, and 0.09 dex for the O3N2 method. Since we are using observations from five different works, which are likely to be affected by diverse observational problems by differing amounts, we argue that this implies that the ONS, C, and N2 methods are the more robust methods. Our comparison of the results implied by the different methods for several of our objects that were also observed by other authors agree with this result. The low dispersions also imply that if there are azimuthal variations in the oxygen abundance in M81, they must be small.

In the case of N/H, we have used the direct method, the C method, and the ONS method, and find gradients of -0.025 to -0.011 dex kpc^{-1}, with the direct method providing again the shallower slope and the largest dispersion around the fit, 0.18 dex, versus 0.15 dex for the ONS method and 0.12 dex for the C method. For N/O we find slopes that go from -0.020 to -0.008 dex kpc^{-1}, with the latter value derived with the direct method, although for this abundance ratio the dispersions are similar for the three methods, 0.11–0.13 dex. The dispersions around the gradients obtained with the different methods for O/H, N/H, and N/O can be qualitatively accounted for by considering the sensitivity of the methods to the two critical line ratios, [N II] $(\lambda 6548 + \lambda 6583)/\lambda 5755$ (our main temperature diagnostic in this work) and [O II] $\lambda 3727/$Hβ.

All the robust methods use the intensity of [N II] $\lambda 6584$, and the N2 method is only based on the intensity of this line with respect to Hα. Since nitrogen and oxygen do not vary in lockstep because they are produced by different types of stars, and their relative abundances depend on the star formation history of the observed galactic region (see e.g. Mollá et al. [2006](#)), the low dispersions around the oxygen abundance gradient found with the robust methods suggest that both N/O and the degree of ionization vary smoothly along the disc of M81. On the other hand, the different values of N/O generally found for regions with similar oxygen abundances imply that strong-line methods that use the intensities of [N II] lines will produce different oxygen abundances in regions that have similar values of O/H but different values of N/O. The ONS and C methods, that use line ratios involving several ions, and also estimate the N/H abundance ratio, can be expected to correct for this effect, at least for regions whose properties are well represented in their calibration samples, but the N2 method by itself cannot achieve this correction. Since our analysis indicates that the available observa-

tions do not allow reliable determinations of abundances through the direct method in this galaxy, and since we do not know if the more robust methods are working properly for the observed H II regions, the magnitude of the metallicity gradient in M81 remains uncertain. These issues should be further investigated using observations of H II regions in different environments that allow the determination of electron temperatures and N and O abundances through the direct method. The large dispersion in the abundances around the gradient that we find here when using the direct method implies that these observations should have high quality in order to get meaningful results. For the time being, we recommend the use of the ONS or C methods when no temperature determinations are possible or when the available determinations are of poor quality.

REFERENCES

Aggarwal K. M., Keenan F. P., 1999, ApJS, 123, 311
Alloin D., Collin-Souffrin S., Joly M., Vigroux L., 1979, A&A, 78, 200
Bresolin F., 2011, ApJ, 730, 129
Bresolin F., Kennicutt R. C. J., Garnett D. R., 1999, A&A, 510, 104
Bresolin F., Gieren W., Kudritzki R.-P., Poetryński G., Urbane M. A., Carraro G., 2009, ApJ, 700, 309
Campbell A., Terlevich R., Manlike J., 1986, MNRAS, 223, 811
Cardelli J. A., Clayton G. C., Mathis J. S., 1989, ApJ, 345, 245
De Robertis M. M., Dufour R. J., Hunt R. W., 1987, J. R. Astron. Soc. Canada, 81, 195
Dopita M. A. et al., 2006, ApJS, 167, 177
Esteban C., Bresolin F., Peimbert M., García-Rojas J., Peimbert A., Mesa-Delgado A., 2009, ApJ, 700, 654
Filippenko A. V., 1982, PASP, 94, 715
Freedman W. L. et al., 2001, ApJ, 553, 47
Garnett D. R., 1992, AJ, 103, 1330
Garnett D. R., Shields G. A., 1987, ApJ, 317, 82
Keenan F. P., Aller L. H., Bell K. L., Hyung S., McKenna F. C., Ramsbottom C. A., 1996, MNRAS, 281, 1073
Kennicutt R. C., Jr, Bresolin F., Garnett D. R., 2003, ApJ, 591, 801
Kewley L. J., Dopita M. A., 2002, ApJ, 142, 35
Kewley L. J., Ellison S. L., 2008, ApJ, 681, 1183
Kong X. et al., 2000, AJ, 119, 2745
Lennon D. J., Burke V. M., 1994, A&AS, 103, 273
Li Y., Bresolin F., Kennicutt R. C., Jr, 2013, ApJ, 766, 17
Liu X. W., Storey P. J., Barlow M. J., Danziger I. J., Cohen M., Bryce M., 2000, MNRAS, 312, 585
López-Sánchez Á. R., Esteban C., 2010, A&A, 517, A85
McCall M. L., Rybski P. M., Shields G. A., 1985, ApJS, 57, 1
Marino R. A. et al., 2013, A&A, 559, A114
Mayya Y. D., Rosa-González D., Santiago-Cortés M., Arellano-Córdova K., Rodríguez M., 2013, Rev. Mex. Astron. Astrofis., 42, 22
Mendoza C., Zeippen C. J., 1982, MNRAS, 198, 127
Mollá M., Vílchez J. M., Gavilán M., Díaz Á. I., 2006, MNRAS, 372, 1069
Ochsendorf B. B., Tielens A. G. G. M., 2015, A&A, 576, A2
Osterbrock D. E., Ferland G. J., 2006, Astrophysics of Gaseous Nebulae and Active Galactic Nuclei, 2nd edn. University Science Books, Sausalito, CA

Pagel B. E. J., Edmunds M. G., Blackwell D. E., Chun M. S., Smith G., 1979, MNRAS, 189, 95

Patterson M. T., Walterbos R. A. M., Kennicutt R. C., Chiappini C., Thilker D. A., 2012, MNRAS, 422, 401

Peña-Guerrero M. A., Peimbert A., Peimbert M., 2012, ApJ, 756, L14

Pérez-Montero E., Contini T., 2009, MNRAS, 398, 949

Pilyugin L. S., 2001a, A&A, 369, 594

Pilyugin L. S., 2001b, A&A, 374, 412

Pilyugin L. S., Thuan T. Z., 2005, AJ, 631, 231

Pilyugin L. S., Vílchez J. M., Contini T., 2004, A&A, 425, 849

Pilyugin L. S., Vílchez J. M., Thuan T. X., 2010, ApJ, 720, 1738

Pilyugin L. S., Grebel E. K., Mattsson L., 2012, MNRAS, 424, 2316

Pilyugin L. S., Grebel E. K., Kniazev A. Y., 2014, A&A, 147, 131

Pradhan A. K., Montenegro M., Nahar S. N., Eissner W., 2006, MNRAS, 366, L6

Rosolowsky E., Simon J. D., 2008, ApJ, 675, 1213

Rubin R. H., 1986, ApJ, 309, 334

Santiago-Cortés M., Mayya Y. D., Rosa-González D., 2010, MNRAS, 405, 1293

Shaw R. A., Dufour R. J., 1995, PASP, 107, 896

Stanghellini L., Magrini L., Villaver E., Galli D., 2010, A&A, 521, A3

Stanghellini L., Magrini L., Casasola V., Villaver E., 2014, A&A, 567, 13

Stasińska G., 1982, A&AS, 48, 299

Stasińska G., 2005, A&A, 434, 507

Stasinska G., 2008, in Hunt L. K., Madden S., Schneider R, eds, Proc. IAU Symp. 255, Low-Metallicity Star Formation: From the First Stars to Dwarf Galaxies, Cambridge Univ. Press, Cambridge, p. 375

Stasinska G., 2010, in Bruzual G., Charlot S., eds, Proc. IAU Symp. Vol. 262, Stellar Populations – Planning for the Next Decade. Cambridge Univ. Press, Cambridge, p. 93

Stauffer J. R., Bothun G. D., 1984, AJ, 89, 1702

Storchi-Bergmann T., Calzetti D., Kinney A. L., 1994, ApJ, 429, 572

Storey P. J., Zeippen C. J., 2000, MNRAS, 312, 813

Tresse L., Maddox S., Loveday J., Singleton C., 1999, MNRAS, 310, 262

van Hoof P. A. M., Weingartner J. C., Martin P. G., Volk K., Ferland G. J., 2004, MNRAS, 350, 1330

Wiese W. L., Fuhr J. R., Deters T. M., 1996, Atomic Transition Probabilities of Carbon, Nitrogen, and Oxygen, American Chemical Society, New York

Zeippen C. J., 1982, MNRAS, 198, 111

SUPPORTING INFORMATION

Additional Supporting Information may be found in the online version of this article:

Table 2. The extinction coefficients $c(H\beta)$ and the reddening-corrected intensities for $H\beta$.

Table 3. Some of the observed and reddening-corrected line ratios, normalized to $I(H\beta) = 100$, for region 1. The error is expressed as a percentage of the reddening-corrected values.

(http://mnras.oxfordjournals.org/lookup/suppl/doi:10.1093/mnras/stv2461/-/DC1).

Please note: Oxford University Press is not responsible for the content or functionality of any supporting materials supplied by the authors. Any queries (other than missing material) should be directed to the corresponding author for the article.

This paper has been typeset from a TEX/LATEX file prepared by the author.